Noise source analysis of porous fairings in a scaled landing gear model

Aerospace Science and Technology 158 (2025) 109885

Contents lists available at ScienceDirect

Aerospace Science and Technology

journal homepage: www.elsevier.com/locate/aescte

Noise source analysis of porous fairings in a scaled landing gear model

R. Zamponi [a,b,*], A. Rubio Carpio [a], F. Avallone [c], D. Ragni [a]

[a] Delft University of Technology, Kluyverweg 1, 2629 HS, Delft, the Netherlands
[b] von Karman Institute for Fluid Dynamics, Waterloosesteenweg 72, B-1640 Sint-Genesius-Rode, Belgium
[c] Politecnico di Torino, Corso Duca degli Abruzzi 24, 10129 Torino, Italy

ARTICLE INFO

Communicated by Antonio Filippone

Keywords:
Landing gear noise
Noise control
Porous fairing
Beamforming
Wind tunnel measurements

ABSTRACT

This paper presents an experimental investigation into the aeroacoustic and aerodynamic impact of various flow-permeable fairings having different levels of airflow resistivity, including wire meshes, perforated plates, and 3D-printed materials based on the repetition of diamond-lattice unit cells. The fairings are installed upstream of a scaled LAGOON landing gear model, which incorporates a torque link and brake-like protuberances to replicate realistic noise sources. Acoustic-imaging measurements carried out on the baseline model reveal that these additional components contribute significantly to far-field acoustic radiation, altering both the location and strength of dominant noise sources. The flow-permeable fairings decrease the model loading and turbulence kinetic energy in its wake compared to a fully solid configuration due to less abrupt flow deflection, with a positive impact on undesired noise possibly arising from interactions with downstream, uncovered gear components. Furthermore, fairings characterized by high airflow resistivity offer comparable or superior sound reductions to the solid fairing within a frequency range where the self-noise produced by the airflow through material pores does not dominate. Beyond generating an extensive dataset to support the validation of numerical simulations, this study provides valuable insight into the development of innovative and more efficient passive sound-control solutions for landing gear systems.

1. Introduction

Among the different contributors to airframe noise, landing gear systems represent the dominant one, accounting for over the 30 % of the overall noise radiated by commercial short-to-medium range aircraft during the approach phase. This source of aerodynamic sound is typically associated with the turbulent wakes detached from the different blunt landing gear sub-components and their interaction with downstream-located gear elements. In particular, the noise radiation from the wheels and the main struts dominates at low and mid frequencies, whereas that produced by smaller elements, such as the hoses and wires linked to the hydraulic system and the small cutouts and steps, dominates at high frequencies [1]. Additionally, tonal-noise contributions are induced by resonant phenomena, mainly occurring on the rims of the wheel cavities [2].

Attempts to mitigate landing gear noise focused on the integration of customized fairings to prevent the interaction of the incoming flow with the gear elements. Dobrzynski et al. [3] achieved overall-sound-pressure-level reductions in the order of 3 dB by installing individual fairings on various components of a realistic Airbus A340 landing gear, such as the tow bar, axle, steering column, upper leg, and wheels. Among these, the bogie-beam undertray fairing was the most effective. Measurements on a 1/4 scale model of the A340's main landing gear, conducted by Li et al. [4], yielded similar sound-mitigation results when scaled up, highlighting the importance of detailed scale-model testing for accurately capturing the impact of high-frequency noise from smaller components. The beneficial effects of customized fairings on the same landing gear model were also confirmed on flight tests by Piet et al. [5], who observed attenuation of 1.8 dB in the effective perceived noise. Similar conclusions were drawn by Ravetta et al. [6], who investigated the impact of multiple fairings mounted on a scaled model of a Boeing 777's main landing gear in wind-tunnel experiments.

Nonetheless, although characterized by a promising sound-control potential, fully solid fairings can induce additional broadband noise sources generated by the high-speed flow deflected by their surface that interacts with surrounding uncovered landing gear components. These sources are expected to scale with the 6th power of the impinging local speed [7] and possibly represent the dominant contributors to the radiated noise given the high Reynolds numbers in real flight [8]. As a consequence, the noise reduction from the shielded components might

* Corresponding author at: Delft University of Technology, Kluyverweg 1, 2629 HS, Delft, the Netherlands.
E-mail address: r.zamponi@tudelft.nl (R. Zamponi).

https://doi.org/10.1016/j.ast.2024.109885
Received 20 September 2024; Received in revised form 13 December 2024; Accepted 16 December 2024

Available online 19 December 2024

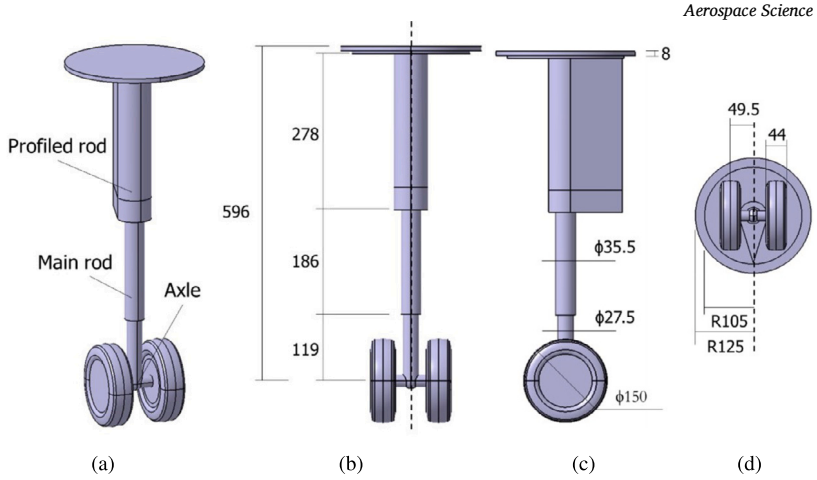

Fig. 1. Sketch of the LAGOON model in the baseline configuration: (a) isometric view; (b) front view; (c) side view; (d) bottom view. Dimensions given in mm.

be counterbalanced by the noise increase from adjacent unshielded elements. Furthermore, besides its effect on the emitted sound, the loading created by the larger impermeable surface exposed to flow produces a higher aerodynamic drag on the landing gear, which is undesirable during take-off. The existing strict requirements of aircraft weight and the necessity for brake cooling may also prevent fully solid fairings from being adopted [9].

Flow-permeable materials were proposed to solve the aforementioned issues [10]. Boorsma et al. [11] demonstrated the noise-mitigation effect of several perforated fairings on the aerodynamic and acoustic performance of a simplified landing gear model, which was associated with the breakdown of the vortex-shedding process. A 18 % reduction in the maximum flow velocity was achieved in that case, resulting in a decrease of unwanted high-speed flow deflection by the fairing. They also observed that excessive porosity values for the material could lead to deterioration in the noise-control potential due to the flow permeating the surface and impinging on the strut. Smith et al. [12] applied porous wire meshes to a scaled model of the main landing gear of a long-range aircraft during approach and concluded that flow-permeable fairings could provide a greater attenuation in the effective perceived noise of more than 3 dB compared to solid configurations with a minimal weight penalty. A similar approach was followed by Oerlemans et al. [13], who installed different types of wire meshes on generic bluff bodies simulating single and combined landing gear components. Promising reductions in the A-weighted overall sound pressure levels in the range of 4 dB to 21 dB were obtained for all tested angles of attack and fairing models. Li et al. [4] assessed the aeroacoustic performance of different solid and porous undertray fairings of a 1/4 scale model of the A340 main landing gear in both closed and open jet wind tunnels. They found that a perforated fairing covered with cloth constituted the most effective replacement for a solid fairing, although no optimization in the perforation geometry was attempted to achieve better mitigation in low-frequency noise and suppress the high-frequency self-noise. Merino-Martínez et al. [14] recently analyzed the sound-control efficiency of several low-noise technologies, including perforated fairings, on a detailed full–scale nose landing gear using 3D acoustic imaging techniques. They confirmed the key role played by the material resistivity in achieving noise mitigation. Nevertheless, no optimal design criteria for porous media were extrapolated in that case.

Despite the numerous studies, the aerodynamic and aeroacoustic alterations induced by porous fairings are yet to be fully clarified [9]. Moreover, the optimal set of porous parameters that maximize noise mitigation while controlling the flow deflection has not yet been identified. The EU H2020 project INVENTOR aims to fill this knowledge gap and develop innovative sound-reduction strategies to decrease the external noise from business-jet and short-to-medium-range transport aircraft. The research work presented in this paper fits within this framework and has the twofold goal of clarifying the noise-generation and attenuation mechanisms induced by flow-permeable fairings installed in a scaled landing gear and generating an extensive dataset that can serve as a validation test case for high-fidelity simulations. Indeed, an enhanced understanding of how these noise sources are affected by the porous materials is instrumental in designing innovative, more effective low-noise solutions, and the insight gained from this study paves the way for optimizing material properties to achieve maximum sound reduction. To the authors' knowledge, no other study in the literature provides such a comprehensive investigation of flow-permeable materials for mitigating landing gear noise.

To pursue this objective, an experimental campaign has been performed at the Delft University of Technology (TU Delft) on a simplified scaled model based on the LAGOON configuration [15], which includes several key elements to make it as representative as possible of a realistic landing gear, such as a torque link and brake-like protuberances. The measurements encompass acoustic beamforming and particle image velocimetry (PIV) to assess the acoustic performance of the different fairing configurations and evaluate their impact on the flow topology around the model. The produced dataset was recently employed to validate the numerical models from Terracol et al. [16], Gondrum et al. [17], and Li et al. [18].

2. Materials and methods

2.1. LAGOON scaled landing gear model

The LAGOON landing gear was originally conceived in the 2000s to create an experimental database for the validation of computational aeroacoustics techniques for airframe noise applications [15]. The model represents a simplified version of a nose landing gear or a direct main landing gear, with the baseline configuration consisting of a profiled rod, a round main rod, a wheel axle, and two wheels with inner rim cavities. It has been extensively investigated within the framework of the BANC workshop series [19].

The mock-up considered in the project INVENTOR, a sketch of which is reported in Fig. 1, is a modified version of the LAGOON model that is scaled down to a wheel diameter of $d_w = 150$ mm, thus having a 1:5 scale with respect to a real nose landing gear, to minimize blockage effects. Additionally, the baseline model can be equipped with representative elements of an Airbus A320 direct-main-landing gear configuration, such as a torque link allocated upstream of the main rod and brake-like protuberances to reproduce most of the noise sources in a real configuration. A picture illustrating these components is reported in Fig. 2. It is worth noting that similar attempts to furnish the LAGOON model with elements mimicking realistic noise sources, i.e., by adding a tow bar, a steering actuator with lights, and a torque link, and removing the wheel

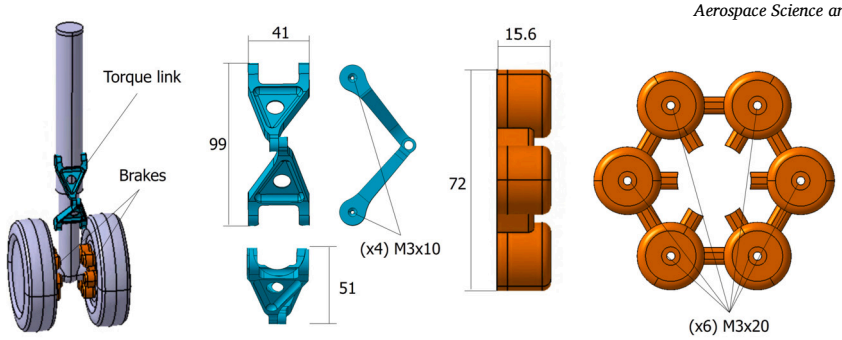

Fig. 2. Sketch of the LAGOON model in the configuration with torque link and brakes. The slots that host the former element are covered with dummy pieces during the baseline measurements. Dimensions given in mm.

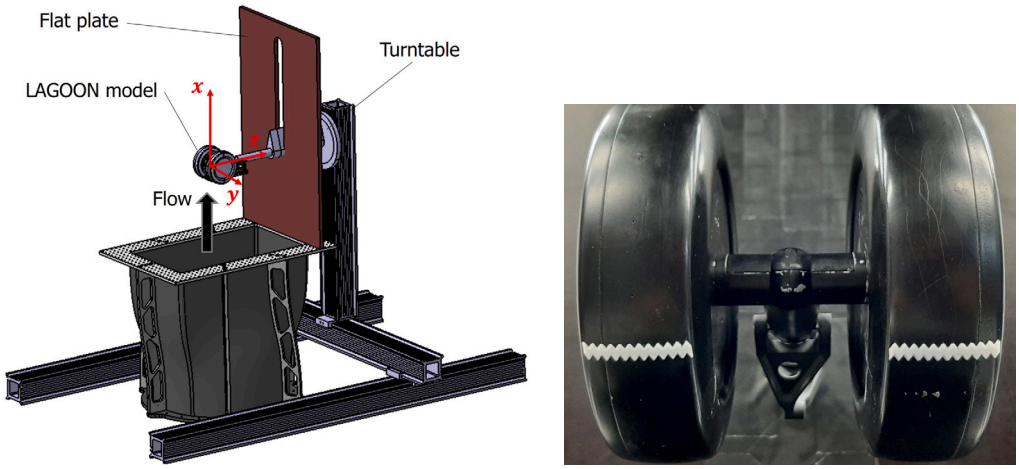

(a) (b)

Fig. 3. (a) Sketch of the experimental set-up designed for the study. (b) Picture of the zig-zag strips applied on the wheels.

rim side caps, were carried out by Sanders et al. [20] and Sengissen et al. [21]. In the latter study, the torque link was installed downstream of the main rod to avoid direct flow incidence.

2.2. Wind tunnel facility

The experiments are conducted at the A-tunnel vertical wind tunnel of TU Delft. The tunnel is an open-jet closed-circuit facility with the test section located in an anechoic plenum with dimensions of $6.4\,\mathrm{m} \times 6.4\,\mathrm{m} \times 3.2\,\mathrm{m}$. The plenum is equipped with Flamex Basic acoustic absorbing foam and features a cutoff frequency of 250 Hz. A detailed description of the facility design is given by Merino-Martínez et al. [22]. The LAGOON model is placed horizontally with the wheel axle at the center of the $0.4\,\mathrm{m} \times 0.7\,\mathrm{m}$ rectangular exit plane of the outlet nozzle. A flat plate is flush mounted to the nozzle exit to mimic the presence of the fuselage belly. The model is attached to the tunnel with a turntable, which allows the adjustment of the yaw angle. A sketch of this setup is illustrated in Fig. 3a, where the reference system considered for presenting the results is also shown. Specifically, the x-axis is aligned with the streamwise direction, the z-axis is aligned with the main-rod axis, and the y-axis is oriented in the normal direction to form a right-handed coordinate system. The origin is set at the intersection between the axis of the wheels and that of the main rod.

The measurements are performed at free-stream flow speeds ranging from $U_\infty = 15\,\mathrm{m\,s^{-1}}$ to $U_\infty = 35\,\mathrm{m\,s^{-1}}$, which correspond to Reynolds numbers based on the wheel diameter of $Re_{d_w} = 1.53 \times 10^5$ and $Re_{d_w} = 3.57 \times 10^5$, respectively. The flow velocity is measured through a Pitot static probe plugged into a Mensor DPG 2400 pressure gauge with an accuracy of 0.03 % of the read value. Zig-zag strips (teeth inclined at 70°, with spacing between two teeth of 3 mm and strip thickness of 0.4 mm) are applied to both sides of each wheel of the model, at ±60° from the stagnation point, to hasten the transition from laminar to turbulent flow (see Fig. 3b). A complete qualification of the outlet nozzle employed in the study was carried out by Merino-Martínez et al. [22], who concluded that the average streamwise velocity could be deemed uniform within 0.6 % independently of the free-stream speed, whereas the turbulence intensity of the clean-flow field was below 0.1 % for the considered speeds.

2.3. Flow-permeable fairings

The LAGOON model can be equipped with a mounting support that can host different types of flow-permeable fairings (Fig. 4). This support is attached directly to the model through the main rod and wheels. This configuration limits the presence of auxiliary struts, which might have a non-negligible effect on the resulting flow and acoustic fields, minimizes vibrations, and mimics the existing support in a real configuration.

The mounting support enables the installation of flat flow-permeable fairings with dimensions of $54\,\mathrm{mm} \times 270\,\mathrm{mm}$ (Fig. 4b, on the left). The fairing covers the wheel axle, brakes, torque link, and the lower part of the main rod. The support allows the installation of porous panels with thicknesses of up to 10 mm. To facilitate the attachment of materials with different microstructures and stiffen the fairing, every porous panel is connected to a light metallic frame (Fig. 4b, on the right), which is screwed to the mounting support. The distance between the outer part of the frame and the main-rod axis d_f can be easily varied between 55 mm and 75 mm. The minimum distance is determined by the presence of the torque link, whereas the maximum one is obtained by aligning the back of the fairing with the front of the wheels.

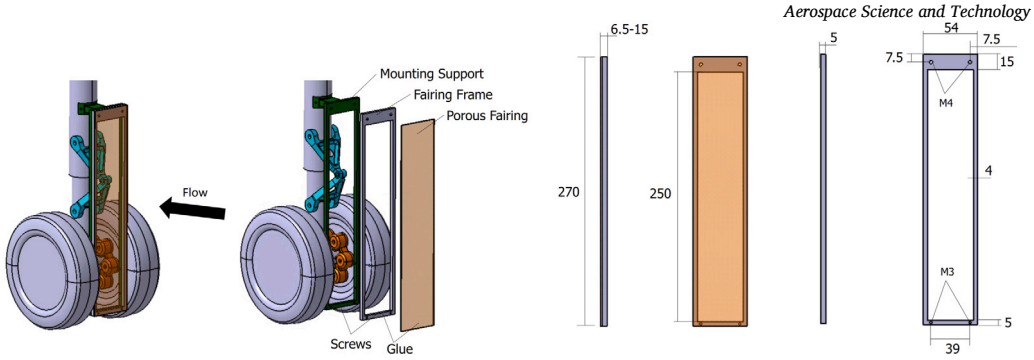

Fig. 4. (a) Mounting support (green), fairing frame (gray), and flow-permeable fairings (orange, translucid) installed on the baseline LAGOON model. (b) Side and front views of porous fairing (on the left) and fairing frame (on the right). Dimensions given in mm. (For interpretation of the colors in the figure(s), the reader is referred to the web version of this article.)

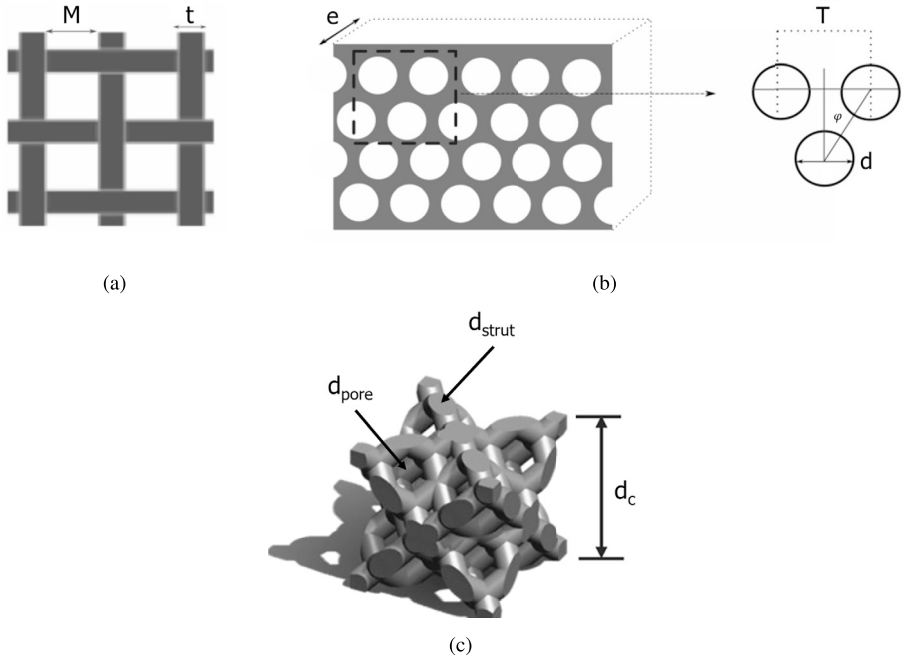

Fig. 5. Schematic of the geometric parameters defining the (a) WM, (b) SCP, and (c) DL fairings.

The present study considers several materials for the porous-fairing design, which can be categorized into three different groups. The first one includes two metallic wire meshes (WM), which differ for mesh size M, wire diameter t, and effective porosity ϕ_{eff}, defined as the ratio of void volume to the total volume (see Fig. 5a). The most permeable is characterized by $M = 4\,\text{mm}$, $t = 1\,\text{mm}$, and $\phi_{\text{eff}} = 64\,\%$ (WM 1), whereas the most resistive by $M = 0.14\,\text{mm}$, $t = 0.042\,\text{mm}$, and $\phi_{\text{eff}} = 59\,\%$ (WM 2).

The second group encompasses perforated plates with straight circular perforations (SCP) having different plate thicknesses e, perforation diameters d, and distances between the centers of two adjacent perforations T (see Fig. 5b). Four combinations of these parameters have been tested, i.e., SCP $d2T3e1$, SCP $d2T3e2$, SCP $d4T6e1$, and SCP $d5T6e1$, and their dimensions are summarized in Table 1.

The third group contains 3D-printed materials that are based on the repetition of diamond-lattice (DL) unit cells with different cell sizes d_c [23]. Each unit cell consists of cylindrical struts with diameters d_{strut} and pore sizes d_{pore}, forming a matrix in a lattice that resembles that of a diamond-atom arrangement and features an effective porosity of $\phi_{\text{eff}} = 61.7\,\%$ (see Fig. 5c). Materials with three different unit-cell dimensions are considered, i.e., $d_c = 2.5\,\text{mm}$ (DL 2.5), 4.5 mm (DL 4.5), and 6.4 mm (DL 6.4). An overview of the geometrical dimensions defining the media and the porous properties is given in Table 2, which additionally lists the static permeability K and the form coefficient C of the material determined using the experimental rig shown by Zamponi et al. [24]. K and C account for pressure losses due to viscous and inertial effects, respectively. These parameters offer a detailed description of the DL-based fairing and can be employed to calibrate porous models in numerical simulations of this experimental setup.

Table 1
Geometric parameters defining the SCP fairings (with reference to Fig. 5b).

Fairing	d (mm)	T (mm)	e (mm)	e/d (-)	ϕ_{eff} (%)
SCP $d2T3e1$	2	3	1	0.5	40.3
SCP $d2T3e2$	2	3	2	1	40.3
SCP $d4T6e1$	4	6	1	0.25	40.3
SCP $d4T6e1$	5	6	1	0.2	62.3

In addition to the aforementioned porous materials, a 3D-printed solid fairing with the same thickness as the DL-based configurations is also manufactured as a reference for comparison purposes. A detailed

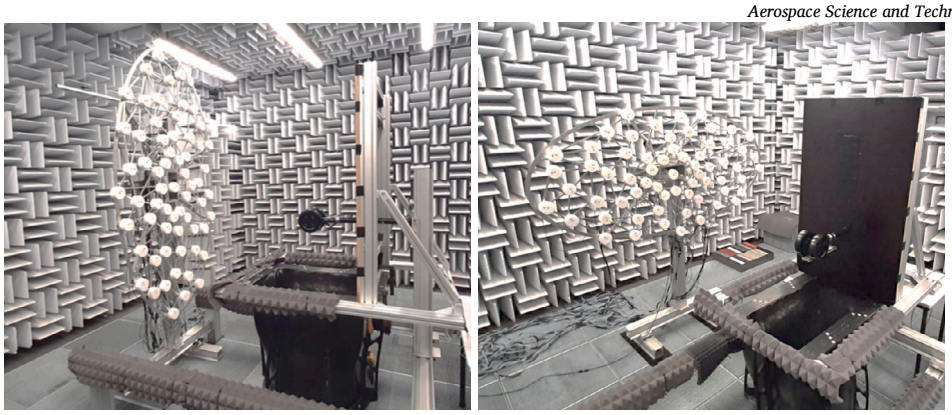

(a) (b)

Fig. 6. Photo of the setup for the acoustic measurements. The microphone array is placed in the (a) flyover and (b) sideline configuration.

Table 2
Geometric parameters defining the DL-based fairings (with reference to Fig. 5c).

d_c (mm)	d_{strut} (mm)	d_{pore} (mm)	K (m^2)	C (m^{-1})
2.5	0.412	0.472	3.019×10^{-9}	1.414×10^{5}
4.5	0.741	0.849	9.160×10^{-9}	6.649×10^{4}
6.4	1.055	1.208	2.016×10^{-8}	2.924×10^{4}

Table 3
Total-pressure drops of the flow through the porous fairings normalized by the dynamic pressure of the inlet velocity of the wind tunnel and evaluated at different downstream distances from the fairing in the streamwise direction.

Inlet velocity (m s^{-1})	16			22		
Downstream distance (mm)	10	40	70	10	40	70
WM 1	0.561	0.608	0.603	0.519	0.596	0.598
WM 2	3.499	4.081	4.279	3.430	3.955	4.205
SCP $d2T3e1$	n/a					
SCP $d2T3e2$	1.900	1.998	2.086	1.925	2.044	2.110
SCP $d4T6e1$	1.670	1.345	1.365	1.731	1.353	1.368
SCP $d5T6e1$	0.494	0.900	0.930	0.478	0.909	0.930
DL 2.5	n/a					
DL 4.5	2.601	2.631	2.666	2.592	2.613	2.655
DL 6.4	2.220	2.312	2.345	2.223	2.280	2.299

investigation of the wake produced by the same porous fairings in the absence of the landing gear model was previously performed by Gallo et al. [25], whereas the characterization of the total-pressure drop experienced by the flow through them at different streamwise distances downstream of the fairings was carried out by Zamponi et al. [26] at the von Karman Institute for Fluid Dynamics. In that case, the fairing width (54 mm) was smaller than that of the wind tunnel test section (250 mm), permitting the flow to be deflected by the surface and mimicking the flow behavior of the present experimental setup. The results of the pressure-drop analysis are reported in Table 3 and give an indication of the resistance experienced by the airflow in permeating the material.

2.4. Far-field acoustic measurements

The far-field aerodynamic noise emitted by the LAGOON model equipped with the different fairing configurations is evaluated using an array of 64 G.R.A.S. 40 PH analog free-field microphones with integrated constant-current power amplifiers. These sensors provide a flat frequency response within ±1 dB from 50 Hz to 5 kHz and within ±2 dB from 5 kHz to 20 kHz. The microphones are plugged into a data acquisition system made of 4 NI PXIe-4499 Sound and Vibration modules with a 24-bit resolution and a 204.8 kHz maximum sampling frequency controlled by a NI RMC-8354 computer via a NI PXIe-8370 board. The amplitude calibration of the transducers is carried out through a G.R.A.S. 42AG piston-phone emitting a sinusoidal wave with an amplitude of 94 dB and at a frequency of 1 kHz.

The microphone array features an aperture of about 2 m and is organized in an optimized multi-arm spiral arrangement [24]. Two different configurations associated with two different views are considered, i.e., *flyover* and *sideline*. In the former, the array is placed 1.05 m away from the LAGOON landing gear and looks at its bottom part (see Fig. 6a). In the latter, it is located at a distance of 1.36 m from the model and has visual access to its side (see Fig. 6b). In that case, the array is rotated 90° to improve the resolution of the noise source localization in the landing gear main-rod direction, i.e., its major axis is horizontal. For each configuration, the array central microphone is approximately aligned with the origin of the reference system. Moreover, the sensors are surrounded by melamine foam disks to attenuate the impact of sound reflections.

Data are acquired at a sampling frequency of 51.2 kHz for 20 s. A total of 3 free-stream flow speeds are investigated, namely $U_\infty = 15\,\mathrm{m\,s^{-1}}$, $25\,\mathrm{m\,s^{-1}}$, and $35\,\mathrm{m\,s^{-1}}$. The power spectral density of the acoustic signals is calculated by means of Welch's method [27] with blocks of 0.1 s that are windowed through a Hanning weighting function with a 50 % data overlap, which leads to a frequency resolution of 10 Hz. The random error linked to this set of parameters amounts to 0.8 dB considering a 95 % confidence interval [28]. The sound pressure levels L_p values are then computed for a reference pressure of $p_{ref} = 20\,\mu\mathrm{Pa}$. Subsequently, an in-house conventional frequency-domain beamforming technique [29] is used to visualize the noise sources produced by the flow interacting with the LAGOON-based model. In addition, corrections to account for the convection of the mean flow and refraction of the shear layer are applied through the method proposed by Sijtsma [30], whereas measurements of the test section without the model are carried out to evaluate the background noise of the wind tunnel.

The scanning grid to assess the potential sources is planar and parallel to the microphone array. For the flyover, it is placed along the wheel axis-streamwise plane and is centered on the origin of the reference system, whereas, for the sideline, it is located in correspondence with the symmetry plane of the landing gear model. The size of the scanning grid is $0.8\,\mathrm{m} \times 0.4\,\mathrm{m}$ and features a spatial resolution of 0.01 m. The source strength from the resulting sound map is then integrated within a predefined region of integration (ROI) to quantitatively determine the radiated noise levels using the source-power-integration (SPI) technique [31]. This method assumes that the integrated source power can be described by a synthetic acoustic monopole, usually placed at the center of the ROI. Therefore, a normalization of the total source power accounting for this elementary source and, consequently, the effects of the microphone array's point spread function [29] is required to scale the integrated power. An extension of $0.4\,\mathrm{m} \times 0.2\,\mathrm{m}$ centered on the origin of the reference system is considered for the ROI, which is sufficiently

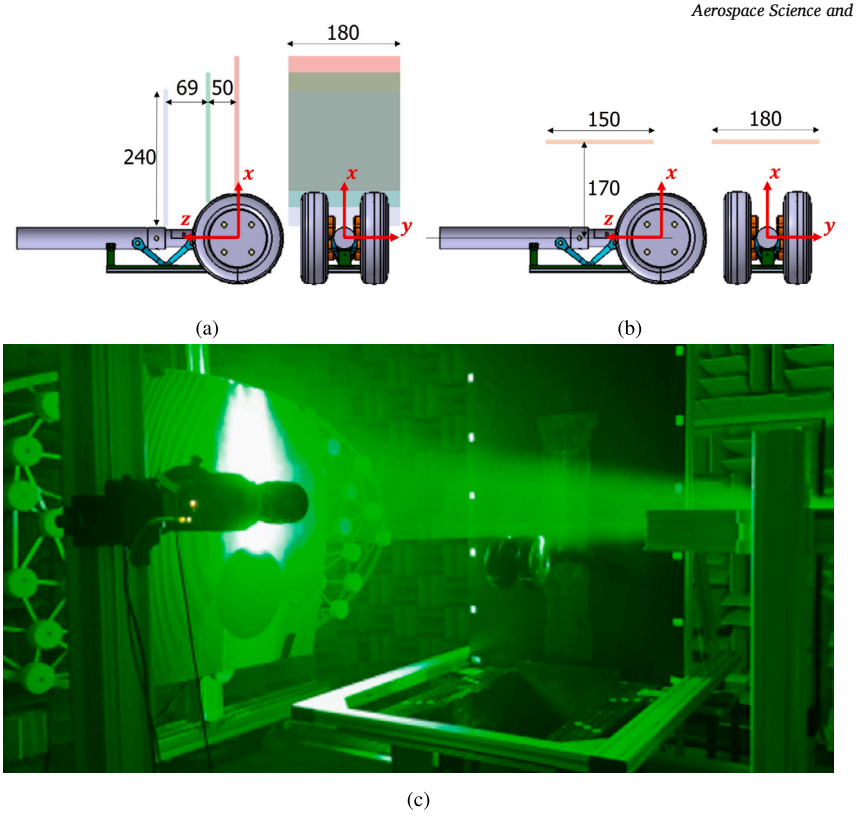

Fig. 7. Dimensions and positions of the FOVS for the (a) x-y planes (2C-PIV) and (b) y-z plane (3C-PIV). (c) Photo of the setup for the 2C-PIV measurements.

wide to encompass the potential main-lobe broadening due to coherence loss with the varying frequency while excluding the contribution of spurious side lobes in the sound map [31].

2.5. Flow-field measurements

The wake flow downstream of the landing gear model is characterized through two-component (2C) and three-component (3C) PIV experiments. 2 LaVision Imager sCMOS cameras with a sensor of 2560 px × 2160 px and pixel pitch of 6.5 µm fitted with Scheimpflug adapters are employed for the experiments. A SAFEX Twin-Fog Double Power fog generator with a SAFEX Long-Lasting glycol mix is used to generate seeding particles featuring mean drop diameters of 0.5 µm. The particles are injected directly into the wind tunnel circuit of the A-Tunnel facility to yield a uniform concentration in the test section. The laser sheet is generated by a Quantel Evergreen 200 double-pulse Nd:YAG system, which emits laser pulses having a wavelength of 532 nm and energy of 200 µJ per pulse. The resulting laser-sheet thickness is approximately 2 mm. A photo of the PIV setup is shown in Fig. 7.

For the 2C-PIV, 1 sCMOS camera is placed at approximately 1 m from the measurement plane and is equipped with a Nikon NIKKOR 60 mm focal-distance macro-objective set at $f_{\#} = 5.6$. The flow field is reconstructed within 3 x-y planes at different spanwise locations (see Fig. 7a). Each field of view (FOV) has a dimension of 0.18 m × 0.24 m and is characterized by a digital resolution of 12 px mm^{-1}, with a magnification factor of 0.078. For the 3C-PIV, the 2 sCMOS cameras forming an angle of 60° are located at about 1.4 m from the measurement plane and feature Nikon NIKKOR 105 mm focal-distance macro-objectives set at $f_{\#} = 11$. The wake flow is reconstructed within 1 y-z plane with dimensions of 0.15 m × 0.18 m placed at 0.17 m from the main rod (see Fig. 7b). The resulting digital resolution is 14.4 px mm^{-1}, with a magnification factor of 0.093.

For each PIV setup, 1000 snapshots per case are acquired using a sampling frequency of 13 Hz. The separation time between two frames is adapted with the objective of ensuring a particle displacement in the free stream of about 12 px. The flow measurements are carried out for a single free-stream flow speed of $U_\infty = 35\,\mathrm{m\,s^{-1}}$ and are performed in the absence of fairings installed on the LAGOON model and for a subset of representative fairing configurations, namely the solid, WM 1, WM 2, SCP $d2T3e2$, DL 2.5, and DL 6.4.

The raw image pairs are processed by means of the commercial software LaVision Davis 10.1.2 using a multi-pass cross-correlation algorithm [32] with a final interrogation window for both PIV setups of 24 px × 24 px and 75 % overlapping, which yields a vector spacing of 0.6 mm and 0.44 mm for the 2C-PIV and 3C-PIV, respectively. The systematic and random components of the PIV uncertainty are evaluated with the method proposed by Wieneke [33], which calculates the differences in the correlation peaks computed from a pair of interrogation windows mapped back onto each other. The uncertainty is then determined by averaging the residuals from the image mapping following Sciacchitano and Wieneke [34]. The maximum error on the mean-velocity magnitude is found to be below the 2 % of the free-field speed for the different considered cases.

3. Results and discussion

3.1. Aeroacoustic results

The representative elements of the Airbus A320 installed on the LAGOON model, namely, the torque link and the brakes, are expected to introduce additional realistic sound sources compared to the baseline configuration. Characterizing these sources is instrumental in clarifying the noise-mitigation mechanisms associated with the fairing. Before delving into the analysis, however, it is important to define a frequency range of interest.

The sound emitted by the landing gear of commercial short-to-medium range aircraft during approach typically dominates for $0.8\,\mathrm{kHz} < f < 3\,\mathrm{kHz}$ [35]. Consequently, low-noise technologies for such systems should focus primarily on this frequency range to effectively contribute to the mitigation of the effective perceived noise of the

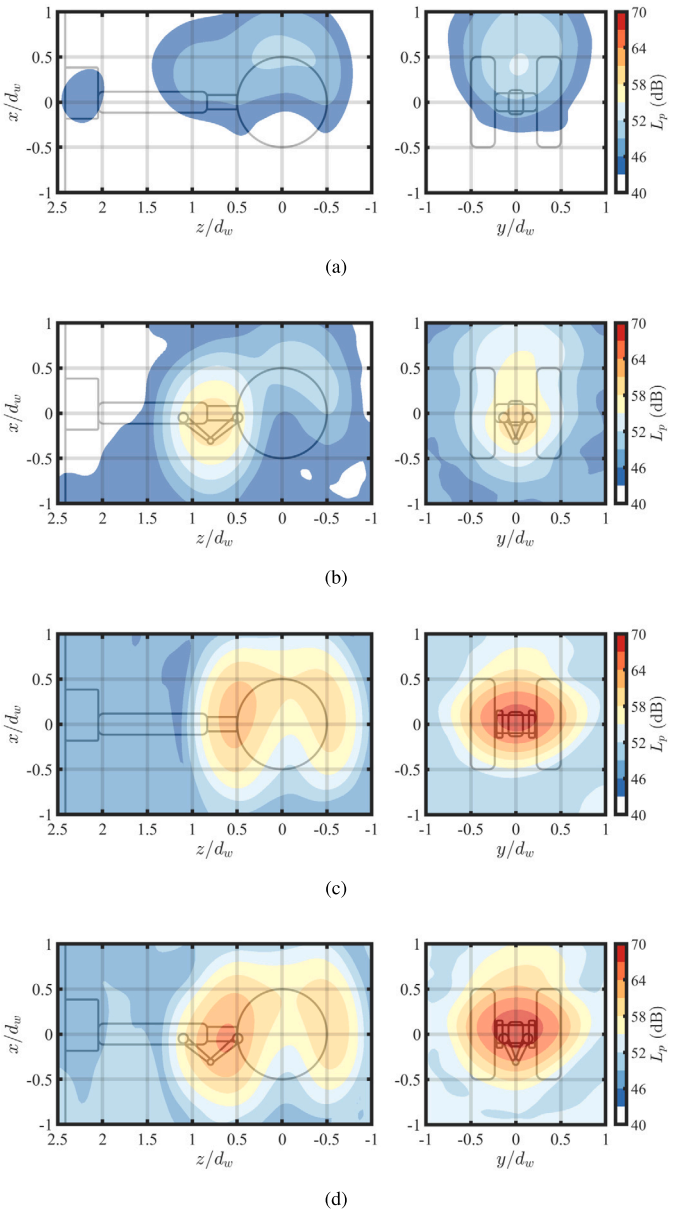

Fig. 8. Sound maps of the LAGOON model computed within $St \in [13.3; 50]$ for the (a) baseline (main rod and wheels), (b) baseline with the torque link, (c) baseline with the brakes, and (d) baseline with the torque link and brakes. Flow going from the bottom to the top of the maps.

aircraft. This range clearly differs when considering the scale of the LAGOON model. Hence, a transposition law based on a Strouhal-number relation is required to relate the model scale and the flow speed in the wind tunnel with the full scale and velocities of short-to-medium range aircraft. Assuming a landing gear diameter wheel of $D_w = 1.2\,\mathrm{m}$ and a reference approach speed of $U_{\mathrm{ref}} = 72\,\mathrm{m\,s^{-1}}$, the Strouhal range of interest in which landing gear noise dominates would be $St \in [13.3; 50]$.

The sound maps for different configurations of the LAGOON model, i.e., the baseline, baseline with only the torque link, baseline with only the brakes, and baseline with both the torque link and brakes, are shown in Fig. 8. All the maps are analyzed using the same dynamic range of 30 dB, and the axes are normalized by the wheel diameter. The maps are computed at the level of the source, implicitly accounting for the varying distances between the microphone array and the scan-grid plane in the two configurations. The results pertain to the Strouhal range of interest and a velocity of $U_\infty = 35\,\mathrm{m\,s^{-1}}$, though similar observations apply to other flow speeds.

For the baseline (Fig. 8a), the dominant noise sources are located near the downstream edges of the wheels, possibly resulting from the scattering of the turbulent wake shed by the main rod and axle. Only one source, centered on the main-rod axis, is detected in this case, which is probably due to the fact that the distance between the wheels, i.e., 55 mm, is smaller than the minimum source-separation distance R that can be resolved by the beamforming method in this frequency range. Indeed, according to the Rayleigh resolution limit [36],

$$R(f) \approx d_{\mathrm{a-s}} \tan\left(\frac{1.22\, c_\infty}{f\, D_a}\right), \tag{1}$$

where $d_{\mathrm{a-s}}$ is the distance between the microphone array and the scan grid, i.e. 1.05 m for the flyover direction, D_a is the array aperture, and f is the frequency being investigated. Considering a minimum frequency of $f = 3.11\,\mathrm{kHz}$, which corresponds to $St = 13.3$, it follows that $R \approx 71\,\mathrm{mm}$. Additionally, the L_p values for the flyover view are notably higher than those for the sideline view due to the partial shielding effect of the wheel closer to the microphone array in the latter setup.

The installation of the torque link (Fig. 8b) leads to a noticeable increase in maximum sound pressure levels of up to 8 dB and a clear shift of the dominant noise source region toward this component, which is caused by the interaction of its turbulent wake with the main rod. The asymmetry of the torque link (see Fig. 2) is reflected in the source distribution, which appears slanted with respect to the y-axis in the flyover direction. Additionally, the absence of a shielding element at this location results in similar L_p values between the flyover and sideline views. In this regard, installing the torque link downstream of the main axis, as done by Sengissen et al. [21], has a potentially beneficial effect on the radiated noise.

Similar considerations apply to the brakes implemented on the baseline (Fig. 8c), although the noise induced by these components is significantly higher. In particular, the L_p peak amplitude increases by approximately 16 dB. The sound scattered at the edges of the wheels is negligible in this case, as are the sound pressure levels recorded by the microphones in the sideline configuration due to the shielding effect of the wheel. The predominant contribution of the brakes to the recorded sound is also observed when these components are installed together with the torque link (Fig. 8d). The additional noise sources produced by the latter element in the Strouhal range of interest are indeed only marginal, suggesting that the considerations made below regarding the effects of different fairing geometries can also be applied to the case where the torque link is positioned downstream of the main rod.

The relative impact of the different configurations can be assessed more quantitatively from the integrated sound spectra for both flyover and sideline directions, which are reported in Fig. 9. In the flyover setup (Fig. 9a), the power spectra exhibit comparable sound pressure levels up to about $St = 2.2$, suggesting that noise is generated by a component included in the baseline configuration. Notably, no distinct vortex shedding-related tonal peak is present throughout the spectrum, although the broadband hump around $St = 4$ seems to be consistent with the Strouhal number at which the onset of round-cavity modes in the fluid volume between the wheels was observed in the original LAGOON model [37]. For $St > 2.2$, the contributions from the torque link and brakes start dominating the radiated sound. Specifically, the spectrum for the LAGOON model equipped with the torque link increasingly deviates from that of the baseline, with a maximum difference of $\Delta L_p = 7\,\mathrm{dB}$ occurring within the Strouhal range of interest. The acoustic effect of the brakes is more significant, corroborating the conclusions drawn from the sound maps. The spectra for the baseline embedding only the brakes feature a peak at approximately $St = 3.8$, which is 12 dB louder than the baseline and might also be related to an acoustic resonance occurring in the cavity between the wheel and excited by a flow instability [38]. Further investigations would be required to clarify this mechanism and attribute the origin of this peak. For $5 < St < 10$ and $St > 30$, brakes and torque link provide comparable contributions, while, for $10 < St < 30$, the noise emitted by the brakes alone dominates the spectrum. This is

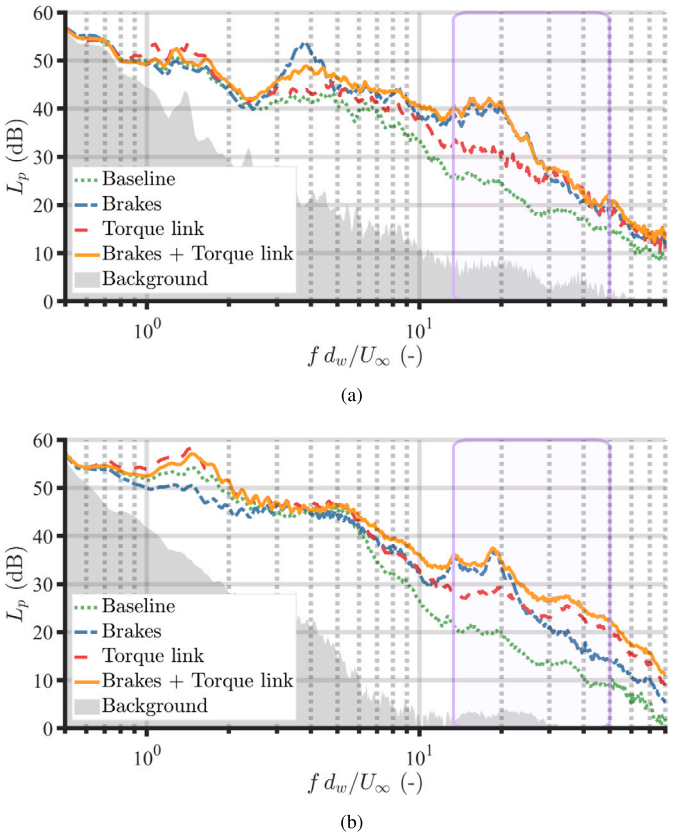

Fig. 9. Integrated sound power spectra in the (a) flyover and (b) sideline setup for the different LAGOON landing gear configurations. In the purple box, the Strouhal range of interest.

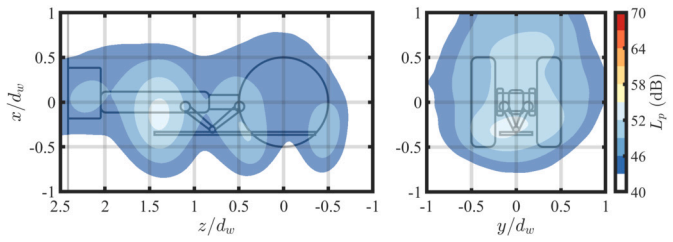

Fig. 10. Sound maps of the LAGOON model equipped with the solid fairing at $d_f = 55$ mm computed within $St \in [13.3; 50]$. Flow going from the bottom to the top of the maps.

likely due to the complex shape of the brakes (see Fig. 2), which induces the detachment of strongly accelerated vortical flow patterns that impinge on the downstream brake protuberances and the wheel surface [16], explaining the source distribution observed in Fig. 8c. Overall, the L_p values computed for the configuration with all the additional components are consistent with the sum of the L_p values of the individual cases. However, the tonal peak at $St = 3.8$ is diminished, suggesting that the presence of the torque link interferes destructively with the noise generated by the brakes.

In the sideline setup (Fig. 9b), the power spectra for both the baseline and the baseline with brakes installed generally exhibit lower values due to the aforementioned shielding effect of the wheel closer to the array. Notably, the peak at $St = 3.8$ observed in the flyover view is no longer visible. As a result, the noise radiated by the torque link becomes predominant for a wider range of Strouhal numbers, specifically for $St < 3$, which may be related to the shedding of vortical structures detached from this component, and $St > 30$. The maximum deviation from the baseline, in this case, amounts to 12 dB around $St = 33$. Despite this, the

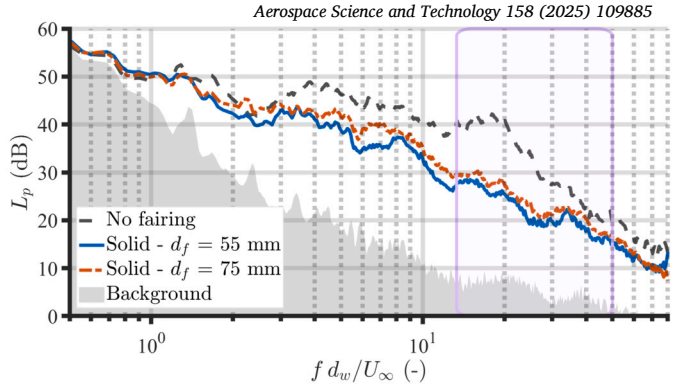

Fig. 11. Integrated sound power spectra in the flyover setup for the LAGOON landing gear model without fairings (including the torque link and brakes) and equipped with the solid fairing at different distances from the main rod. In the purple box, the Strouhal range of interest.

contribution of the sound generated by the brakes still dominates in the Strouhal range of interest, as the source-distribution maps in Figs. 8c and 8d also show.

These results confirm the rationale for using fairings as sound-mitigation technologies for landing gear systems. By covering the torque link and brakes, they are expected to prevent the flow from interacting with these components, which provides the largest contribution to the sound spectrum. To verify this point, the sound maps for the model equipped with a solid fairing placed at a distance of $d_f = 55$ mm in the flyover and sideline directions are shown in Fig. 10. As in previous cases, the maps are computed within the Strouhal range of interest. In the sideline view, the dominant noise sources are produced by the flow detaching from the upper part of the fairing and impinging on the main rod, at approximately $z = 0.2$ m. Additional secondary sources are located in the vicinity of the upstream edges of the wheels. In the flyover direction, sound originates from the region between the fairing and the main rod, likely generated by the interaction of flow detached from the sides of the solid surface with the two wheels. Furthermore, sources near the downstream edges of the wheels are visible again, albeit with lower amplitude. Overall, the L_p values for both views are comparable to those observed for the baseline, underscoring the beneficial acoustic impact of the fairing.

A more quantitative assessment of the noise-mitigation performance of the solid fairing is provided in Fig. 11, which shows the integrated sound power spectra for the LAGOON model equipped with this component in the flyover setup. Two different distances of the fairing from the main rod are analyzed, namely $d_f = 55$ mm and $d_f = 75$ mm. The spectra are compared to those of the baseline configuration with the torque link and brakes included. The noise reduction provided by the solid fairing extends across the entire spectrum, particularly in the Strouhal range of interest, with significant deviations of up to 16 dB around $St = 20$. Moreover, similar values of ΔL_p are also observed when the fairing is placed farther from the main rod, suggesting that most of the acoustic benefits of the device come from deflecting the flow outside the inter-wheel region. Yet, a noise increase of up to 4 dB is noted for $d_f = 75$ mm in the range $5 < St < 8$, which may be linked to a stronger interaction of the flow detached at the edges of the relatively large solid surface with the main rod due to the higher velocities. This is because the L_p values of landing gear components increase with the 6th power of the local incident flow speed [7]. Therefore, a smaller d_f is more beneficial for the sound-mitigation performance of this technology. In the subsequent analysis, a fixed distance corresponding to $d_f = 55$ mm will be considered.

The effect of the different flow-permeable materials on the radiated noise is now examined in comparison with the solid fairing and the baseline LAGOON model fitted with the torque link and brakes. The power spectra for the wire meshes WM1 and WM2 in the flyover direction are

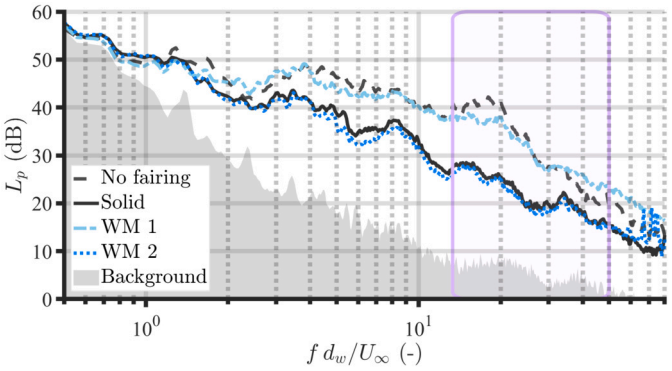

Fig. 12. Integrated sound power spectra in the flyover setup for the LAGOON landing gear model equipped with the solid and WM fairings at $d_f = 55$ mm. In the purple box, the Strouhal range of interest.

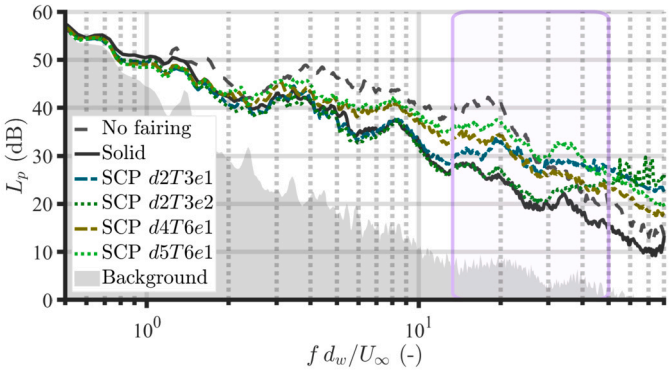

Fig. 13. Integrated sound power spectra in the flyover setup for the LAGOON landing gear model equipped with the solid and SCP fairings at $d_f = 55$ mm. In the purple box, the Strouhal range of interest.

shown in Fig. 12. WM1 is nearly ineffective at reducing the noise radiated by the model, exhibiting only a marginal reduction of up to 4 dB at approximately $St = 18$ and increase for $St > 32$. Conversely, WM2 outperforms the sound-mitigation potential of the solid fairing, achieving reductions of up to 4 dB around $St = 5$. In the Strouhal range of interest, in particular, the difference between the solid and porous fairing configurations lies in the order of 2 dB. This result can be attributed to the differing permeability values of the wire meshes. Indeed, WM1 features a very low resistivity, making it almost transparent to the incoming velocity (see Table 3), while WM2 has high resistance to the flow, comparable to that of the DL fairings, thereby weakening its interaction with the downstream components of the model.

In the case of the SCP plates, the noise reduction with respect to the baseline equipped with the torque link and brakes is not consistent across the frequency spectrum. The power spectra for the flow-permeable fairings in this family, which are visible in Fig. 13 in the flyover direction, are similar to those of the solid configuration for low frequencies and diverge at higher frequencies. SCP $d4T6e1$ and SCP $d5T6e1$ begin to deviate at $St = 5$ and follow the same trend up to $St = 10$. Above this threshold, SCP $d5T6e1$ produces higher L_p values, surpassing the baseline LAGOON model without a fairing from $St = 28$ onward. $St = 10$ is also the Strouhal number from which SCP $d2T3e1$ starts increasingly deviating from the solid configuration. SCP $d2T3e2$ shows the best noise-reduction performance in the Strouhal range of interest since its sound emissions are comparable to those of the solid one up to $St = 25$, owing to the higher total-pressure drop induced by this material (see Table 3). In view of the above, the geometric characteristics of the perforations significantly influence the sound-mitigation capability of the fairing. Smaller diameters and larger thicknesses provide the best performance, with thickness appearing to be the most

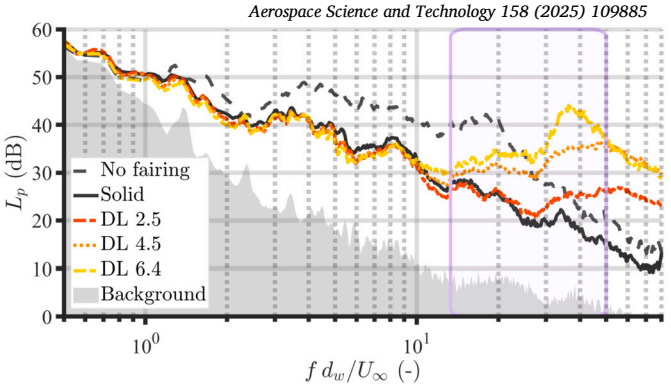

Fig. 14. Integrated sound power spectra in the flyover setup for the LAGOON landing gear model equipped with the solid and DL fairings at $d_f = 55$ mm. In the purple box, the Strouhal range of interest.

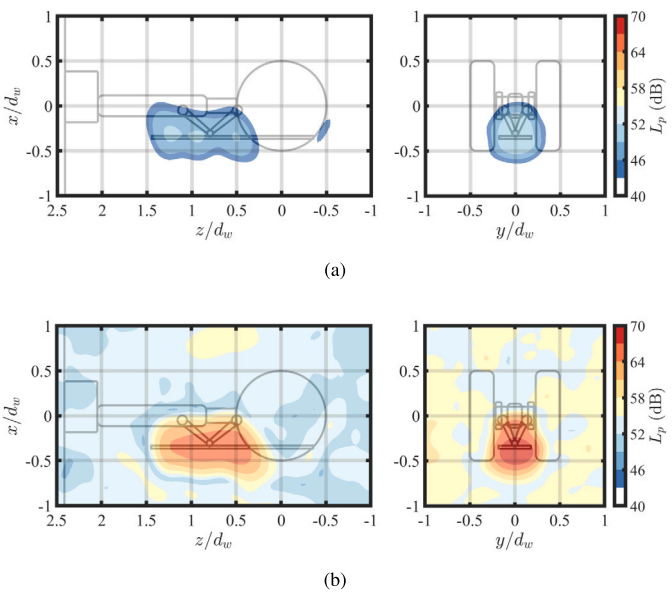

Fig. 15. Sound maps of the LAGOON model equipped with (a) DL 2.5 and (b) DL 6.4 at $d_f = 55$ mm computed within $St \in [33.3; 50]$. Flow going from the bottom to the top of the map.

critical factor. Additionally, the increase in noise at higher Strouhal numbers is likely due to fairing self-noise caused by flow recirculating within the pores of the plate [4], which typically occurs for porous surfaces exposed to airflow. In this case, a larger pore diameter results in a lower frequency at which self-noise starts to dominate.

The comparison of the power spectra for the DL fairings with the reference configurations is shown in Fig. 14 for the flyover setup. A preliminary version of these results was recently presented by Bennett et al. [35]. The higher resistivity of the DL materials compared to the SCP plates yields L_p values slightly lower than those of the solid fairing up to $St = 10$, with no discernible effect of the characteristic dimension of the unit cell on the radiated sound. Above this Strouhal number, the trends for the different DL materials significantly change due to material self-noise, which is more pronounced for the more permeable fairings. Notably, DL 2.5 exhibits a trend similar to SCP $d2T3e2$ in Fig. 13 within the Strouhal range of interest. For $St > 30$, all DL materials are louder than the no-fairing configuration, with a peak increase of $\Delta L_p = 19$ dB observed for DL 6.4. A clearer view of the fairing self-noise is provided in Fig. 15, which presents sound maps for the LAGOON model fitted with DL 2.5 and DL 6.4 over the integrated Strouhal range of $30 < St < 50$. In both cases, the dominant noise source is located across the exposed fairing surface, supporting the hypothesis that the noise is generated by

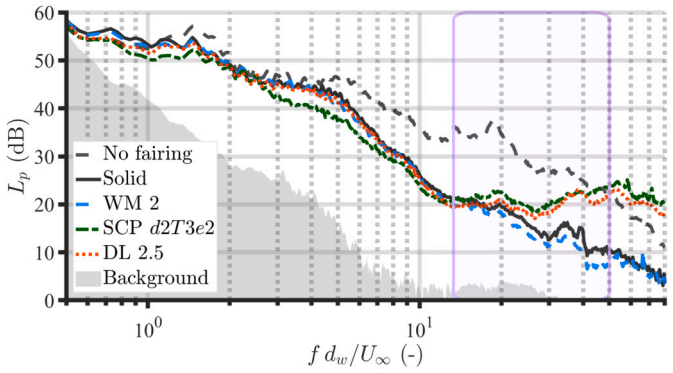

Fig. 16. Integrated sound power spectra in the sideline setup for the LAGOON landing gear model equipped with different fairing configurations at $d_f = 55$ mm. In the purple box, the Strouhal range of interest.

flow interacting within the pores of the material. Notably, the radiated sound displays higher amplitude levels in the flyover direction.

Finally, similar considerations apply to the sideline setup. For the sake of conciseness, only the most effective fairings for each family, i.e., the most resistive ones, will be compared in this view. The corresponding power spectra are shown in Fig. 16. Interestingly, SCP $d2T3e2$ provides better sound reduction than the solid fairing for $2.5 < St < 8$, with attenuation of up to 6 dB. Such a result suggests that this perforated plate influences the noise generated by the interaction of flow detached from the upper edge of the material with the main rod (see Fig. 10). Similar to the flyover setup, WM 2 and DL 2.5 perform as if they were impermeable to flow, but only the former achieves a sound reduction of up to 4 dB with respect to the solid fairing in the Strouhal range of interest, making it the best-performing material among all tested configurations.

3.2. Aerodynamic results

The characterization of the flow past the LAGOON model aims to complement the acoustic study and assess the aerodynamic alterations produced by the different fairings, which have implications for the noise radiated due to the interaction of their wake with downstream gear elements (see Section 1). Moreover, the permeability of the porous material is expected to impact the loading caused by the additional surface area exposed to the flow, thereby affecting the drag exerted on the landing gear system. In this regard, the velocity distributions of the wake flow obtained from the PIV are representative of the momentum deficit induced by the fairing, which is, in turn, linked to drag.

The average streamwise velocity $\overline{u}$ and turbulence kinetic energy k, defined as $k = 0.5\,(u_{\text{rms}}^2 + v_{\text{rms}}^2)$, with u_{rms} and v_{rms} being the root-mean-square values of the velocity fluctuations along the x and y axes, respectively, are qualitatively shown in Fig. 17 for the LAGOON model in the absence of fairings. Once again, the results refer to $U_\infty = 35\,\text{m s}^{-1}$, but similar considerations can be made for the other flow speeds. For the baseline configuration (Figs. 17a and 17b), the flow downstream of the main rod resembles that of a solid circular cylinder [24], with a recirculation region near the aft part of the body and well-defined shear layers delimiting the wake in which turbulence kinetic energy is concentrated. Yet, the noise associated with this vortex-shedding phenomenon is not deemed to be dominant, as observed in Fig. 9. A low-velocity region is also found behind the wheels and axle, indicating turbulence mixing, while the flow accelerates in correspondence with the side of the wheels.

When the torque link is installed (Figs. 17c and 17d), the wake downstream of the main rod becomes wider, and the shear layers diffuse over a longer distance due to the mixing of the turbulent structures shed by this component. This flow-field alteration also affects the adjacent low-velocity region, inducing lower values of $\overline{u}$ and k with respect to the baseline in the mid x-y plane. A clear extension in the recirculation re-

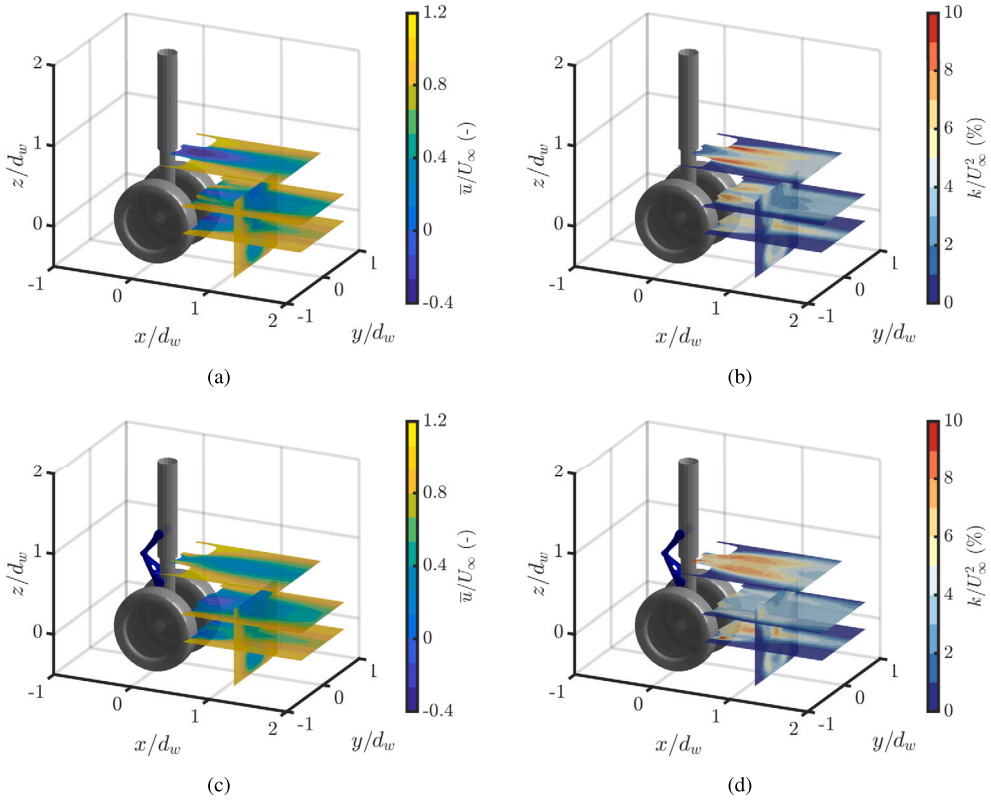

Fig. 17. Normalized (a, c, e, g) average streamwise velocity and (b, d, f, h) turbulence kinetic energy of the LAGOON model for the (a, b) baseline (main rod and wheels), (c, d) baseline with the torque link, (e, f) baseline with the brakes, and (g, h) baseline with the torque link and brakes.

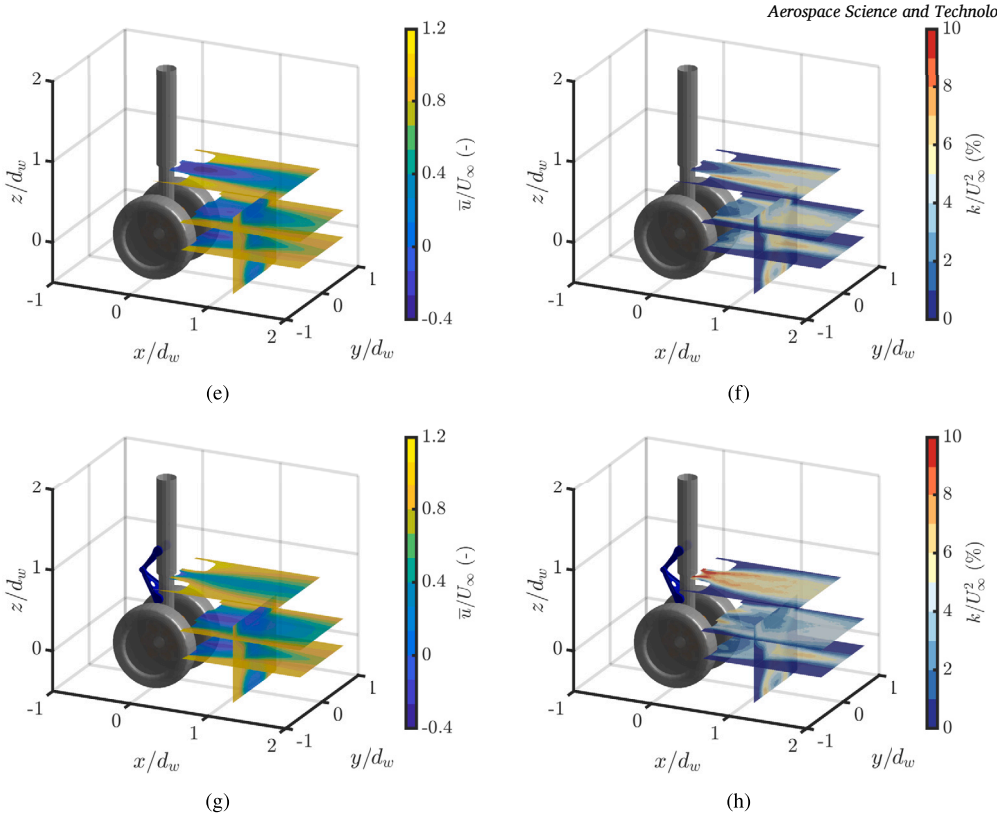

Fig. 17. (*continued*)

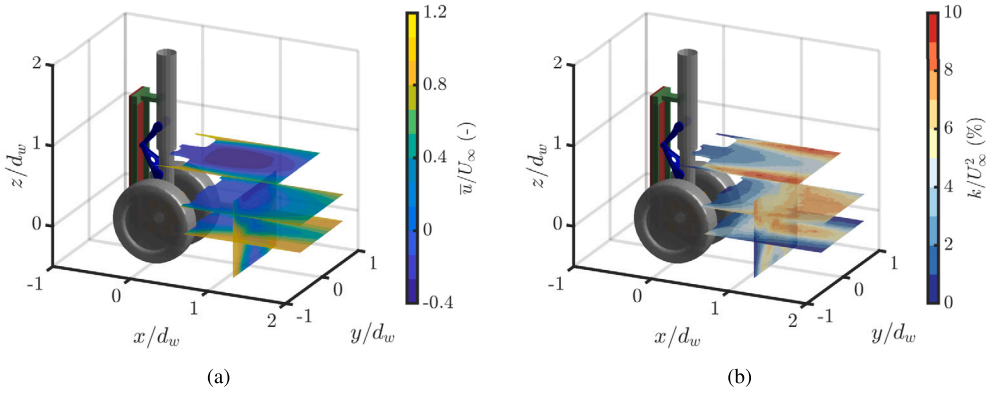

Fig. 18. Normalized (a) average streamwise velocity and (b) turbulence kinetic energy of the LAGOON model equipped with the solid fairing. The flow speed is $U_\infty = 35\,\mathrm{m\,s^{-1}}$.

gion behind the wheels and an increase in turbulence kinetic energy in this region are observed for the baseline including the brakes (Figs. 17e and 17f). The combination of these trends characterizes the flow past the baseline equipped with both the torque link and brakes (Figs. 17g and 17h). In this case, the torque link exhibits the most significant impact on the turbulent wake induced by the LAGOON model when these components are not shielded.

The scenario pictured above changes drastically when the solid fairing is present. The $\overline{u}$ and k fields for this configuration are shown in Fig. 18. In this case, the wake features an extended recirculation region located downstream of the main rod, after which the flow that initially detaches from the sides of the impermeable plate reattaches [25]. Similar to the previous case, the absence of a distinctive low-frequency peak in Fig. 11 suggests that the vortex-shedding noise associated with this flow behavior is not dominant. The more slanted shear-layer angles indicate a greater deflection of the flow and a significant increase in the pressure drag exerted by the model. Overall, the wake is characterized by substantially higher values of turbulence kinetic energy spread over a wider area compared to the case with no fairing.

When the material is porous, the extent of the low-velocity region downstream of the model generally decreases, as do the corresponding k values due to the reduced deflection caused by the flow-permeable surface. These trends can be observed in Fig. 19, which illustrates the average streamwise velocity and turbulence kinetic energy evaluated in the x-y FOV at $z/d_w = 0.793$ for different flow-permeable fairings with respect to the solid case. Profiles of these contour plots extracted at a representative location of $x/d_w = 1$ are shown in Fig. 20 for a more quantitative evaluation. The flow field for WM1 (Figs. 19c and 19d) confirms that this mesh is nearly transparent to the incoming velocity and does not prevent the interaction of high-speed flow with the model components, although it decreases the k values in the wake compared to the baseline with torque link and brakes installed (see Fig. 17h). In

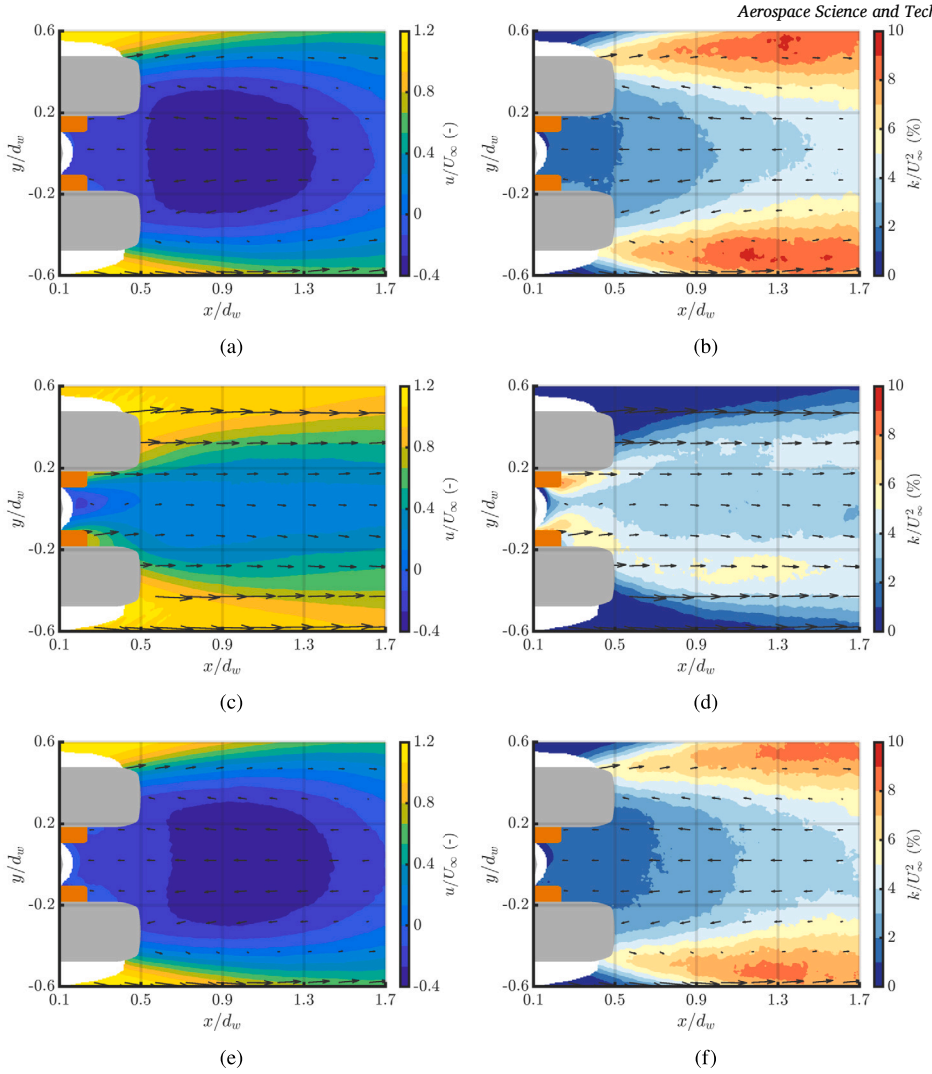

Fig. 19. Normalized (a, c, e, g, i, k) average streamwise velocity and (b, d, f, h, j, l) turbulence kinetic energy of the LAGOON model equipped with (a, b) the solid fairing, (c, d) WM1, (e, f) WM2, (g, h) SCP $d2T3e2$, (i, j) DL 2.5, and (k, l) DL 6.4 on a x-y plane located at $z/d_w = 0.793$.

contrast, WM2 (Figs. 19e and 19f) induces a similar flow deflection to the solid configuration, with slight mitigation in turbulence kinetic energy within the shear layers. Interestingly, SCP $d2T3e2$ yields a more positive contribution to the downstream-flow topology of the LAGOON model, substantially reducing the shear-layer angles, i.e., the flow deflection, and the turbulence production in the wake with respect to the solid fairing. This trend is even more pronounced for DL 6.4 (Figs. 19k and 19l), owing to the high permeability that characterizes this material (see Table 2). The more resistive DL 2.5 (Figs. 19i and 19j), on the other hand, exhibits similar $\overline{u}$ and k trends to WM2, confirming the direct link between airflow resistivity and extent of the recirculation region. These results demonstrate that an optimization of the porous properties of the fairing to obtain significant noise mitigation while controlling the wake flow is possible.

4. Conclusion

The present research paper investigates the acoustics and flow topology of fairings with varying levels of airflow resistivity as passive low-noise and flow-control technologies for a simplified landing gear model, which incorporates representative elements of a direct-main-landing gear configuration, such as the torque link and brakes. The results show that the acoustic impact of these realistic elements, evaluated in a frequency range where landing gear noise prevails for commercial short-to-medium range aircraft, is significant. Moreover, their presence substantially affects the location and strength of the dominant noise sources, i.e., the sound-generation mechanisms. The installation of a solid fairing preventing the flow from interacting with these components leads to remarkable noise reductions of up to 16 dB in both flyover and sideline directions. In this case, the impingement of high-speed flow abruptly separated from the solid material on the main rod of the landing gear model becomes the predominant sound-production mechanism. The larger the distance between the fairing and the main rod is, the more significant this source of noise will be. Nevertheless, the impermeable surface also induces a substantially higher blockage on the incoming flow, increasing the pressure drag exerted by the model and the turbulence kinetic energy in its wake. As a consequence, potential noise sources are generated by the interaction of the wake flow with downstream elements, which may prevail considering the high Reynolds number involved in real flight.

Several flow-permeable fairings are investigated and compared with the solid case, such as wire meshes, perforated plates, and 3D-printed structures based on the repetition of a unit cell. For all the tested cases, it emerges that the best-performing materials in terms of sound-mitigation potential are those that offer the highest resistance to the airflow, i.e., the least permeable ones, in agreement with the literature. In this perspective, the possibility for the flow to permeate the material does not yield additional acoustic benefits regarding the aerodynamic interac-

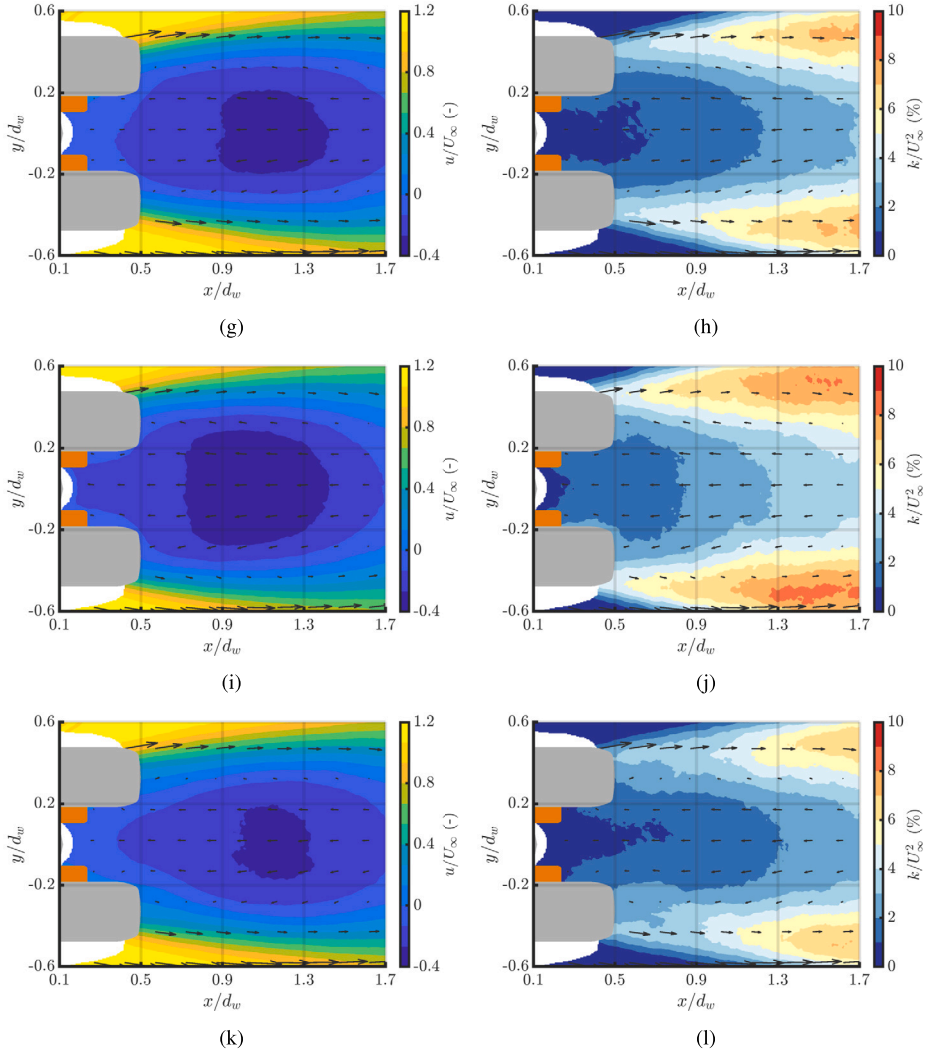

Fig. 19. (*continued*)

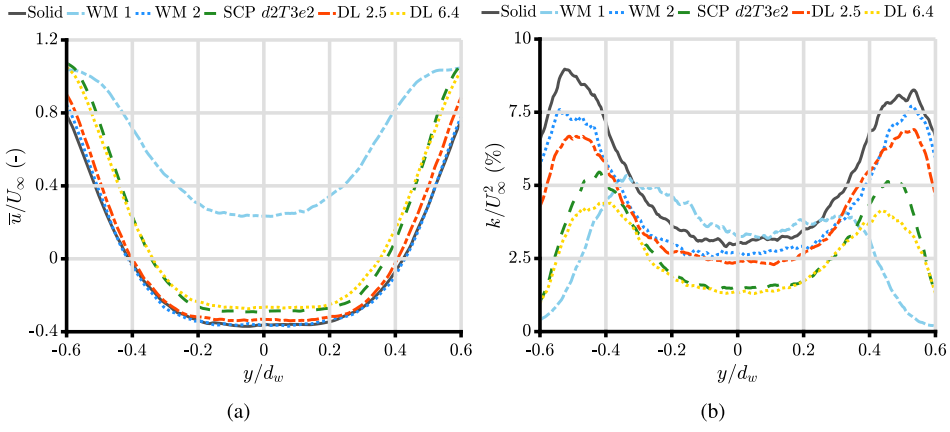

Fig. 20. Normalized (a) average streamwise velocity and (b) turbulence kinetic energy of the LAGOON model equipped with the different fairings extracted at $x/d_w = 1$ and $z/d_w = 0.793$.

tion with the landing gear components but potentially weakens the impingement of the separated flow on the main rod. The resulting noise reductions are indeed comparable or slightly superior to the solid configuration provided that the self-induced sound generated by the flow interacting within the pores of the permeable surface does not dominate. The frequency at which this trade-off occurs, as well as the amplitude of the high-frequency noise increase, depends on the porous characteristics of the medium. In particular, the smaller the pore diameter and the thicker the material, the better the sound-mitigation capability of the fairing. Furthermore, all the tested materials have a positive impact on the wake flow of the model, i.e., they induce a lower pressure drag and decrease the turbulence kinetic energy compared to the solid configu-

ration. This is caused by the less abrupt flow deflection at the sides of the fairing, which potentially lowers undesired interaction noise originating from downstream uncovered gear components while minimizing the additional weight of the model.

To optimize the design of a landing gear fairing, several key considerations must be addressed. First, achieving a trade-off between sound reduction and wake-flow control is critical. This requires careful tuning of the material permeability, which should be low enough to prevent the impingement of high-velocity flow on the brakes and torque link, and high enough to make the flow deflection at the fairing surface more streamlined. Second, the self-noise generated by flow interacting within the pores of the fairing significantly impacts the overall radiated sound, hindering the sound-decrease potential of this technology. The geometry of the porous material, particularly its surface characteristics, affects the frequency at which these noise sources become dominant and their strength. Materials with small pore diameters are preferable as they shift noise sources to higher, potentially inaudible frequencies [8]. Moreover, the regular pore spacing and orientation of the materials tested in this study suggest that tailoring permeability distribution could further improve performance. A non-uniform design might better guide the flow and reduce its interaction with the main rod and downstream gear components. In this regard, the option of 3D-printing flow-permeable materials based on the repetition of a unit cell is particularly attractive, as it allows for precise control over the permeability distribution and geometric customization owing to the recent advancements in additive manufacturing techniques.

Finally, the extensive dataset generated from the LAGOON model in this study also serves as a valuable validation test case for further research on the topic. One of the objectives of the INVENTOR project is to improve the capability of current numerical tools to adequately simulate landing gear flows in the presence of porous devices. The very small pores of the porous media compared to the size of the landing gear system make their direct resolution extremely difficult to perform due to computational limitations [16]. Dedicated macroscopic numerical models need thus to be developed and validated to this end, and the availability of high-quality wind tunnel data can support this research path.

CRediT authorship contribution statement

R. Zamponi: Writing – original draft, Visualization, Software, Methodology, Investigation, Formal analysis, Conceptualization. **A. Rubio Carpio:** Writing – review & editing, Visualization, Validation, Methodology, Investigation, Formal analysis, Data curation, Conceptualization. **F. Avallone:** Writing – review & editing, Supervision, Resources, Project administration. **D. Ragni:** Writing – review & editing, Supervision, Project administration, Funding acquisition.

Declaration of competing interest

The authors declare that they have no known competing financial interests or personal relationships that could have appeared to influence the work reported in this paper.

Acknowledgements

This project has received funding from the European Union's Horizon 2020 Research and Innovation Programme, in the framework of the project INVENTOR (INnoVative dEsign of iNstalled airframe componenTs for aircraft nOise Reduction) listed under the grant agreement ID: 860538. The authors thank ONERA, DLR, and Dassault Aviation for providing the wire meshes and SCP samples tested in this study.

Data availability

Data will be made available on request.

References

[1] Y. Guo, A statistical model for landing gear noise prediction, J. Sound Vib. 282 (2005) 61–87, https://doi.org/10.1016/j.jsv.2004.02.021.
[2] T.R. Ricciardi, W.R. Wolf, N.J. Moffitt, J.R. Kreitzman, P. Bent, Numerical noise prediction and source identification of a realistic landing gear, J. Sound Vib. 496 (2021) 115933, https://doi.org/10.1016/j.jsv.2021.115933.
[3] W. Dobrzynski, L. Chow, P. Guion, D. Shiells, Research into landing gear airframe noise reduction, in: 8th AIAA/CEAS Aeroacoustics Conference & Exhibit, American Institute of Aeronautics and Astronautics, Breckenridge, CO, 2002.
[4] Y. Li, M. Smith, X. Zhang, Measurement and control of aircraft landing gear broadband noise, Aerosp. Sci. Technol. 23 (2012) 213–223, https://doi.org/10.1016/j.ast.2011.07.009.
[5] J.F. Piet, R. Davy, G. Elias, H. Siller, L. Chow, C. Seror, F. Laporte, Flight test investigation of add-on treatments to reduce aircraft airframe noise, in: 11th AIAA/CEAS Aeroacoustics Conference, American Institute of Aeronautics and Astronautics, Monterey, CA, 2005.
[6] P. Ravetta, R. Burdisso, W. Ng, Wind tunnel aeroacoustic measurements of a 26%-scale 777 main landing gear, in: 10th AIAA/CEAS Aeroacoustics Conference, American Institute of Aeronautics and Astronautics, Manchester, UK, 2004.
[7] M. Smith, L. Chow, Validation of a prediction model for aerodynamic noise from aircraft landing gears, in: 8th AIAA/CEAS Aeroacoustics Conference & Exhibit, American Institute of Aeronautics and Astronautics, Breckenridge, CO, 2002.
[8] Y. Li, X. Wang, D. Zhang, Control strategies for aircraft airframe noise reduction, Chin. J. Aeronaut. 26 (2013) 249–260, https://doi.org/10.1016/j.cja.2013.02.001.
[9] K. Zhao, P. Okolo, E. Neri, P. Chen, J. Kennedy, G.J. Bennett, Noise reduction technologies for aircraft landing gear - a bibliographic review, Prog. Aerosp. Sci. 112 (2020) 100589, https://doi.org/10.1016/j.paerosci.2019.100589.
[10] W. Dobrzynski, L.C. Chow, M. Smith, A. Boillot, O. Dereure, N. Molin, Experimental assessment of low noise landing gear component design, Int. J. Aeroacoust. 9 (2010) 763–786, https://doi.org/10.1260/1475-472X.9.6.763.
[11] K. Boorsma, X. Zhang, N. Molin, L.C. Chow, Bluff body noise control using perforated fairings, AIAA J. 47 (2009) 33–43, https://doi.org/10.2514/1.32766.
[12] M. Smith, L. Chow, N. Molin, Control of landing gear noise using meshes, in: 16th AIAA/CEAS Aeroacoustics Conference, American Institute of Aeronautics and Astronautics, Stockholm, SE, 2010.
[13] S. Oerlemans, C. Sandu, N. Molin, J.-F. Piet, Reduction of landing gear noise using meshes, in: 16th AIAA/CEAS Aeroacoustics Conference, American Institute of Aeronautics and Astronautics, Stockholm, SE, 2010.
[14] R. Merino-Martínez, J. Kennedy, G.J. Bennett, Experimental study of realistic low–noise technologies applied to a full–scale nose landing gear, Aerosp. Sci. Technol. 113 (2021) 106705, https://doi.org/10.1016/j.ast.2021.106705.
[15] E. Manoha, J. Bulté, B. Caruelle, Lagoon: an experimental database for the validation of CFD/CAA methods for landing gear noise prediction, in: 14th AIAA/CEAS Aeroacoustics Conference (29th AIAA Aeroacoustics Conference), American Institute of Aeronautics and Astronautics, Vancouver, BC, 2008.
[16] M. Terracol, E. Manoha, L. Manueco, F. Avallone, D. Ragni, A. Rubio Carpio, Numerical simulations of a landing gear with flow through fairings for noise mitigation, in: AIAA AVIATION 2023 Forum, American Institute of Aeronautics and Astronautics, San Diego, CA, 2023, Online.
[17] M. Gondrum, M. Meinke, W. Schroeder, F. Avallone, D. Ragni, Porous fairings for landing gear noise mitigation, in: 30th AIAA/CEAS Aeroacoustics Conference (2024), American Institute of Aeronautics and Astronautics, Rome, IT, 2024.
[18] S. Li, L. Davidson, S.-H. Peng, A.R. Carpio, D. Ragni, F. Avallone, A. Koutsoukos, On the mitigation of landing gear noise using a solid fairing and a dense wire mesh, Aerosp. Sci. Technol. (2024) 109465, https://doi.org/10.1016/j.ast.2024.109465.
[19] E. Manoha, B. Caruelle, Summary of the LAGOON solutions from the benchmark problems for airframe noise computations-III workshop, in: 21st AIAA/CEAS Aeroacoustics Conference, American Institute of Aeronautics and Astronautics, Dallas, TX, 2015.
[20] L. Sanders, E. Manoha, S. Ben Khelil, C. François, CFD/CAA coupling on the LAGOON #2 landing gear using a structured multi-block solver with the Chimera technique, in: 19th AIAA/CEAS Aeroacoustics Conference, American Institute of Aeronautics and Astronautics, Berlin, DE, 2013.
[21] A. Sengissen, J.-C. Giret, C. Coreixas, J.-F. Boussuge, Simulations of LAGOON landing-gear noise using Lattice Boltzmann Solver, in: 21st AIAA/CEAS Aeroacoustics Conference, American Institute of Aeronautics and Astronautics, Dallas, TX, 2015.
[22] R. Merino-Martínez, A. Rubio Carpio, L.T. Lima Pereira, S. van Herk, F. Avallone, D. Ragni, M. Kotsonis, Aeroacoustic design and characterization of the 3D-printed, open-jet, anechoic wind tunnel of Delft University of Technology, Appl. Acoust. 170 (2020) 107504, https://doi.org/10.1016/j.apacoust.2020.107504.
[23] C. Teruna, F. Avallone, D. Ragni, A. Rubio-Carpio, D. Casalino, Numerical analysis of a 3-D printed porous trailing edge for broadband noise reduction, J. Fluid Mech. 926 (2021) A17, https://doi.org/10.1017/jfm.2021.704.
[24] R. Zamponi, F. Avallone, D. Ragni, C. Schram, S. Van Der Zwaag, Relevance of quadrupolar sound diffraction on flow-induced noise from porous-coated cylinders, J. Sound Vib. 583 (2024) 118430, https://doi.org/10.1016/j.jsv.2024.118430.
[25] E. Gallo, R. Zamponi, A. Zarri, Y.C. Kucukosman, C. Schram, Experimental characterization of flow through porous fairings, in: AIAA AVIATION 2023 Forum, American Institute of Aeronautics and Astronautics, San Diego, CA, 2023, Online.

[26] R. Zamponi, E. Gallo, A. Zarri, J. De Decker, Y.C. Küçükosman, C. Schram, Characterization of the flow through innovative permeable fairings at the VKI WAABLIEF facility, https://doi.org/10.5281/ZENODO.7220605, 2022.

[27] P. Welch, The use of fast Fourier transform for the estimation of power spectra: a method based on time averaging over short, modified periodograms, IEEE Trans. Audio Electroacoust. 15 (1967) 70–73, https://doi.org/10.1109/TAU.1967.1161901.

[28] A. Brandt, Noise and Vibration Analysis: Signal Analysis and Experimental Procedures, John Wiley & Sons, 2011.

[29] C.S. Allen, W.K. Blake, R.P. Dougherty, D. Lynch, P.T. Soderman, J.R. Underbrink, Aeroacoustic Measurements, Springer Berlin Heidelberg, 2002.

[30] P. Sijtsma, Phased Array Beamforming Applied to Wind Tunnel and Fly-Over Tests, Technical Report, National Aerospace Laboratory, 2010.

[31] R. Merino-Martínez, P. Sijtsma, A. Rubio Carpio, R. Zamponi, S. Luesutthiviboon, A. Malgoezar, M. Snellen, C. Schram, D. Simons, Integration methods for distributed sound sources, Int. J. Aeroacoust. 18 (2019) 444–469, https://doi.org/10.1177/1475472X19852945.

[32] F. Scarano, M.L. Riethmuller, Advances in iterative multigrid PIV image processing, Exp. Fluids 29 (2000) S051–S060, https://doi.org/10.1007/s003480070007.

[33] B. Wieneke, PIV uncertainty quantification from correlation statistics, Meas. Sci. Technol. 26 (2015) 074002, https://doi.org/10.1088/0957-0233/26/7/074002.

[34] A. Sciacchitano, B. Wieneke, PIV uncertainty propagation, Meas. Sci. Technol. 27 (2016) 084006, https://doi.org/10.1088/0957-0233/27/8/084006.

[35] G.J. Bennett, J. Lai, G. O'Brien, D. Ragni, F. Avallone, M. Pott-Pollenske, Flow control and passive low noise technologies for landing gear noise reduction, in: 28th AIAA/CEAS Aeroacoustics 2022 Conference, American Institute of Aeronautics and Astronautics, Southampton, UK, 2022.

[36] L. Rayleigh, Investigations in optics, with special reference to the spectroscope, Lond. Edinb. Dublin Philos. Mag. 8 (1879) 261–274.

[37] D. Casalino, A.F.P. Ribeiro, E. Fares, S. Nölting, Lattice–Boltzmann aeroacoustic analysis of the LAGOON landing-gear configuration, AIAA J. 52 (2014) 1232–1248, https://doi.org/10.2514/1.J052365.

[38] T.R. Ricciardi, W.R. Wolf, R. Speth, Acoustic prediction of LAGOON landing gear: cavity noise and coherent structures, AIAA J. 56 (2018) 4379–4399, https://doi.org/10.2514/1.J056957.